


FULL PAPER

Open Access



Estimation of the emission altitude of pulsating aurora using the five-wavelength photometer

Yuki Kawamura^{1*} , Keisuke Hosokawa¹, Satonori Nozawa², Yasunobu Ogawa³, Tetsuya Kawabata², Shin-Ichiro Oyama^{2,3,4}, Yoshizumi Miyoshi², Satoshi Kurita⁵ and Ryoichi Fujii²

Abstract

Using a ground-based five-wavelength photometer, which has been operative in Tromsø, Norway since February 2017, we have statistically analyzed the lifetime of $O(^1S)$ to reveal the emission altitude of pulsating aurora (PsA). For the statistics, we have extracted intervals of PsA using an EMCCD all-sky imager on 37 nights during 3 months from January to March, 2018. By performing a cross-correlation analysis between the time-series of 427.8 nm (N_2^+ first negative band) and 557.7 nm oxygen emissions, we derived the distribution of the lifetime of $O(^1S)$. The mean of the lifetime is 0.67 s and the mode is around 0.7 s. We estimated the emission altitude of PsA using the lifetime of $O(^1S)$ and then carried out a case study, in which we compared the temporal variations of the emission altitude with the peak height of E region ionization obtained from the simultaneous observation of the EISCAT UHF radar. We confirmed an overall agreement between the two parameters, indicating the feasibility of using the current method for estimating the energy of precipitating electrons causing PsA. In addition, we have derived the statistical characteristics of the emission altitude of PsA. The result shows that the emission altitude becomes lower in the morning side than in the midnight sector, which indicates that the energy of PsA electrons is higher in the later MLT sector. Especially, there is a decrease of the emission altitude at around 06 MLT. However, the model calculation infers that the energy of cyclotron resonance between magnetospheric electrons and whistler-mode chorus waves does not change so much depending on MLT. This implies that the observed change of the emission altitude cannot be explained only by the MLT dependence of resonance energy.

Keywords: Ionosphere, Pulsating Aurora, Cyclotron resonance, Ground-based optical observation

Introduction

Pulsating aurora (PsA) is a category of diffuse aurora, which is characterized by luminosity blinking with a periodicity ranging from a few to a few tens of seconds (Yamamoto 1988). Such a quasi-periodic luminosity variation is called the main pulsation [(Hosokawa et al. 2015) and reference therein]. PsAs are generally observed in the morning side during the recovery phase of auroral substorms (Kvifte and Pettersen 1969). They often continue

for a few hours or longer (Jones et al. 2011). The spatial structure of PsA is divided into the following two broad categories: (1) cluster of patches with irregular shapes (patch-type) and (2) bundles of arcs elongating mostly in the east–west direction (arc-type) (Royrvik and Davis 1977; Yamamoto 1988; Sato et al. 2004).

The temporal variation of PsA is associated with quasi-periodic precipitation of energetic electrons from the magnetosphere (e.g., Sandahl et al. 1980). Previous studies have suggested that such quasi-periodic precipitations are caused by the wave–particle interaction between whistler-mode chorus waves and ambient electrons whose energy ranges from a few to a few tens of

*Correspondence: yukikawamura@uec.ac.jp

¹ University of Electro-Communications, Chofugaoka 1-5-1, Chofu, Tokyo 182-8585, Japan

Full list of author information is available at the end of the article

keV [e.g., (Miyoshi et al. 2010, 2015a, b)]. Especially, it has been reported that there is a one-to-one correspondence between the amplitude variation of chorus waves and the luminosity modulation of PsA (Nishimura et al. 2010, 2011). These observational results imply that PsA is the two-dimensional projection of the characteristics of chorus waves in the magnetosphere. Although recent literatures, which analyzed the simultaneous ground-satellite observations, have revealed the correspondence between PsA and chorus waves (e.g., Kasahara et al. 2018; Hosokawa et al. 2020), it is still unclear what factors control these periodic variations.

The emission altitude of PsA has been studied intensively since 1970s using optical data from ground-based all-sky video cameras (e.g., Brown et al. 1976). The altitude of PsA emission contains information about the energy of precipitating electrons, which allows us to infer the nature of wave-particle interaction process. Thus, there have been many studies investigating the altitude of PsA and the energy of precipitating electrons. Brown et al. (1976) estimated the lower cut-off altitude of PsA emission through triangulation of two all-sky TV cameras having a common field-of-view. They showed that the height of PsA emission ranges from 82 to 115 km; corresponding energy of electrons being from 50 to 5 keV, respectively, which is consistent with direct in situ observations of PsA electrons by sounding rockets (e.g., Sandahl et al. 1980). However, Brown et al. (1976) analyzed only 2 h of optical observations from 3 nights. Recently, similar analysis by Partamies et al. (2017) demonstrated that the height of PsA becomes slightly lower in the morning sector. But, it is still unclear whether this trend is statistically significant due to the limited amount of data available. Jones et al. (2009) estimated the energy of PsA electrons from ionospheric electron density observations by the Poker Flat Incoherent Scatter Radar (PFISR). More recently, Hosokawa and Ogawa (2015) studied the variation of electron density profile during PsA using the European Incoherent SCATter (EISCAT) radar. They demonstrated that the energy of PsA electrons, inferred from the altitude of ionization, tends to be higher in the morning side (i.e., in the later MLT sector). Miyoshi et al. (2015a) identified a few hundred keV electron precipitations during simultaneous measurements of PsA with EISCAT and Van Allen Probes. Then, they proposed a model explaining the scattering of electrons in a wide range of energy by considering the propagation of chorus waves toward higher latitudes.

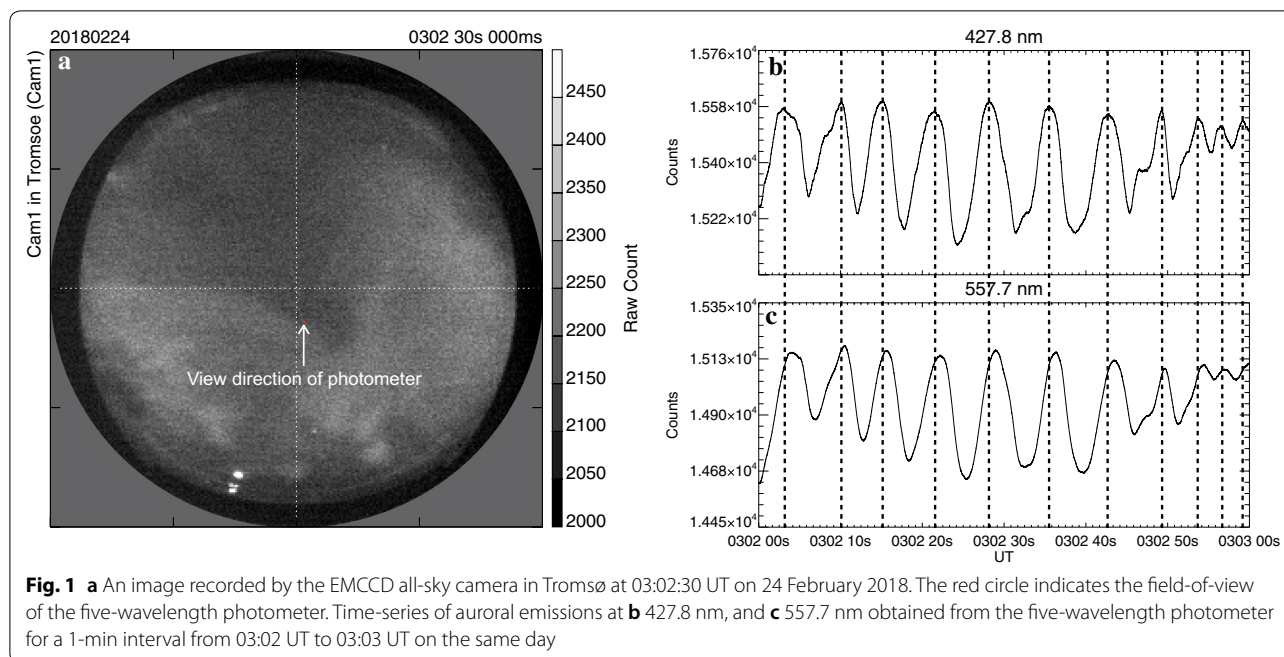
As mentioned above, ionospheric electron density variations during PsA have been studied in detail using incoherent scatter radars. In the past, however, the MLT dependence of the altitude of PsA has not been examined using a sufficient amount of data. Thus far, the

statistical properties of the energy of PsA electrons are still unknown. To solve this problem, we need a method that can derive the altitude of PsA emission in a statistical manner. Scourfield et al. (1971) proposed a procedure for estimating the emission altitude of PsA using the lifetime of $O(^1S)$ excited state atoms seen in the optical observations. Since the transition from $O(^1S)$ to $O(^1D)$ producing 557.7 nm emission is forbidden and its lifetime is about 0.70 s, time-series of the 557.7 nm emission exhibits a systematic time lag compared to that of an allowed transition emission such as 427.8 nm, whose lifetime is $\sim 10^{-8}$ s (Nozawa et al. 2018). Scourfield et al. (1971) estimated the altitude of the 557.7 nm emission from this delay time because the delay time is longer at higher altitudes. Their method has a potential to estimate the energy of PsA electrons. However, Scourfield et al. (1971) only proposed the above-mentioned method, which has not actually been used for the statistical analysis of the altitude of PsA.

In this paper, we performed a statistics by applying the method of Scourfield et al. (1971) to multi-wavelength photometer observations in Tromsø, Norway. This approach enables us to derive the statistical characteristics of the emission altitude of PsA, which provides fundamental information about the energy of PsA electrons and wave-particle interaction process in the magnetosphere.

Datasets

In the current statistical analysis, we employed the five-wavelength photometer (Nozawa et al. 2018) and Electron Multiplying Charged Coupled Device (EMCCD) all-sky camera both of which have been operative in Tromsø, Norway (69.6N, 19.2E, 66.7MLAT). The five-wavelength photometer has the field-of-view (FOV) of about 0.98 degrees and measures the auroral emissions in the field-aligned direction at 5 wavelengths simultaneously (427.8 nm, 557.7 nm, 630.0 nm, 777.4 nm, 844.6 nm). The original sampling rate is 400 Hz. The EMCCD all-sky camera mainly observes N_2 first positive band emissions with a temporal resolution of 100 Hz. These temporal resolutions are sufficiently high to detect the main pulsation of PsA whose periodicity ranges from a few to a few tens of seconds. In this study, we employed images from the all-sky camera to identify the appearance of PsA at the sensing point of the photometer. Figure 1 introduces a typical example of PsA during a 1-min interval from 03:02 to 03:03 universal time (UT) on 24 February 2018. Figure 1a shows an image from the all-sky camera at 03:02:30 UT. The red circle gives the FOV of the photometer. Figure 1b and c shows the time-series of the emission intensity from the photometer at the 427.8 nm and 557.7 nm wavelengths, respectively. Note



that both the time-series have already been averaged with an integration time of 1 s to improve the signal-to-noise ratio. The quasi-periodic fluctuation, whose periodicity is about 5 s, is obvious in the time-series. It is also seen that there is a systematic time lag between the 427.8 nm and 557.7 nm emissions. By comparing data from these two optical instruments, we identified 37 nights of PsA events during 3 months from January to March, 2018, which were used for the current statistical analysis.

Methodology for estimating the lifetime of $O(^1S)$

Before showing the statistical results, we introduce the methodology for estimating the lifetime of $O(^1S)$ using the case of PsA shown in Fig. 2. In this study, we calculate the lifetime of $O(^1S)$ every 1 min by performing cross-correlation analysis between the time-series of the 427.8 nm and 557.7 nm emissions. We decided to use relatively short (1 min) time intervals for the correlation analysis, to eliminate unwanted contributions of slower variations. Figure 2a and b again shows the time-series of the 427.8 nm and 557.7 nm emissions from the same interval shown in Fig. 1. It is clearly seen that the time-series of 557.7 nm has a time delay of 1 s or less as compared to that of 427.8 nm. Here, we define the lifetime of $O(^1S)$ as a time lag giving the maximum cross-correlation coefficient. Note that the correlation coefficient is calculated by shifting the lag from 0 to 2 s with a resolution of 0.01 s, the time window of analysis being 30 s. The result of the correlation analysis is shown in Fig. 2c, where the dashed line gives the time-series of 557.7 nm and the

solid line shows the time-shifted (i.e., delayed by the estimated time lag) variation of 427.8 nm. In this case, the lifetime of $O(^1S)$ is estimated to be 0.67 s as a lag giving a maximum correlation coefficient of 0.99.

Statistics of distribution of the lifetime of $O(^1S)$

Figure 3a shows the distribution of lifetime of $O(^1S)$ derived by applying the above-mentioned procedure to 2856 events of PsA each of which has a duration of 1 min. The distribution has a prominent peak (mode) at around 0.7 s and the mean of the distribution is 0.67 s. Brekke and Henriksen (1972) also calculated the lifetime of $O(^1S)$ using a photometer which operated in Tromsø, Norway. In their result, the lifetime was distributed from 0.5 to 1 s and the mean was 0.80 s. Our result shows general agreement with that of Brekke and Henriksen (1972). In our case, however, the mean value is slightly shorter than that in their statistics. The time window for the cross-correlation analyses of Brekke and Henriksen (1972) was 5 min whereas the present study uses a window of 1 min duration. This difference might have introduced the slight difference between these two statistics. However, when we carried out the cross-correlation analysis using several different time windows, no significant differences were found; thus, the reason for the difference is still unclear at this stage.

We classified events by magnetic local time (MLT) and investigated the MLT dependence of the lifetime of $O(^1S)$. The results are summarized in Fig. 3b–d. Those panels respectively show the distributions of the lifetime

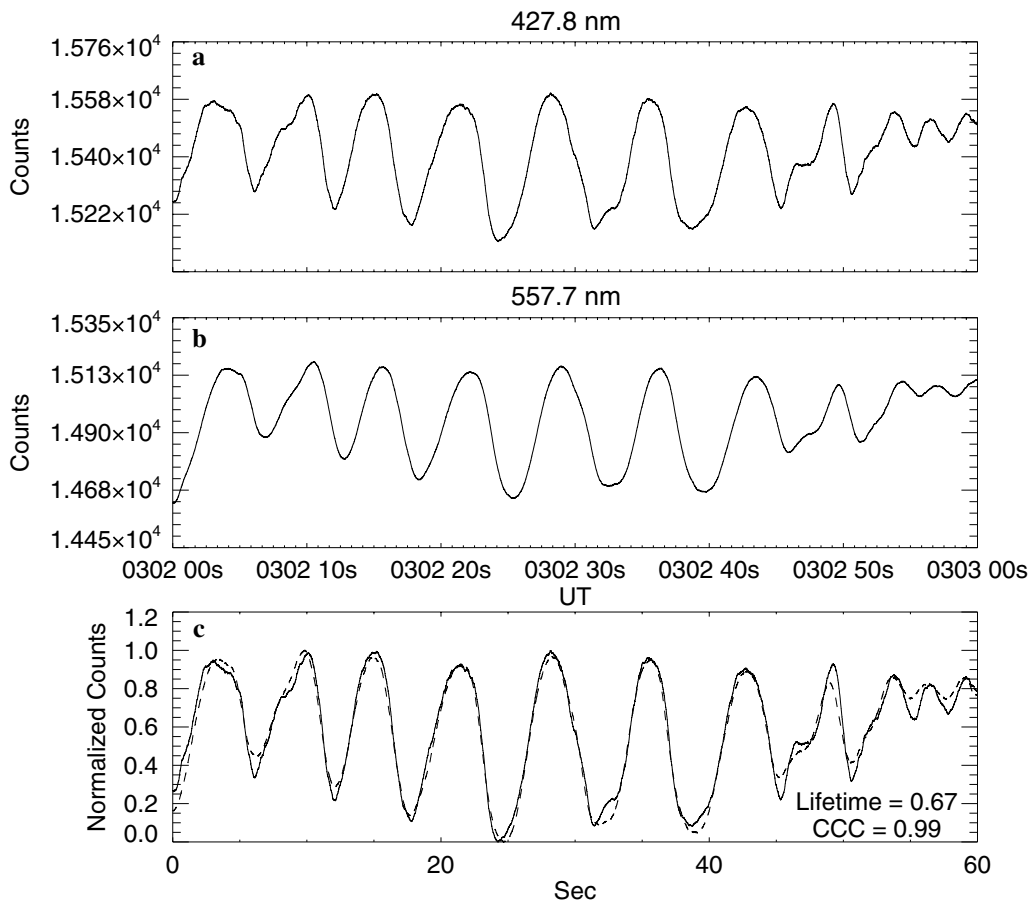


Fig. 2 Time-series of auroral emissions at **a** 427.8 nm and **b** 557.7 nm observed at Tromsø for a 1-min interval from 03:02 UT to 03:03 UT on 24 February 2018. **c** Comparison of the two time-series of the 557.7 nm (dashed line) and 427.8 nm (solid line) emissions. The time-series of the 427.8 nm is delayed by 0.67 s, which corresponds to the lifetime of O(¹S)

in three MLT sectors, i.e., 20-03 MLT, 03-05 MLT, and 05-08 MLT. The mode and mean of the lifetime are respectively 0.70 and 0.70 s for 20-03 MLT, 0.65 and 0.69 s for 03-05 MLT, and 0.50 and 0.64 s for 05-08 MLT. In addition, when focusing on the shape of the distribution, the weight is shifted to the shorter area in the morning side. In particular, for the 05-08 MLT case (Fig. 3d), there is a significant population having a lifetime of about 0.60 s, which is not seen before 05 MLT (Fig. 3b, c). In the following section, we will estimate the altitude of PsA emission from these values of lifetime.

Calculating the effective altitude of pulsating aurora

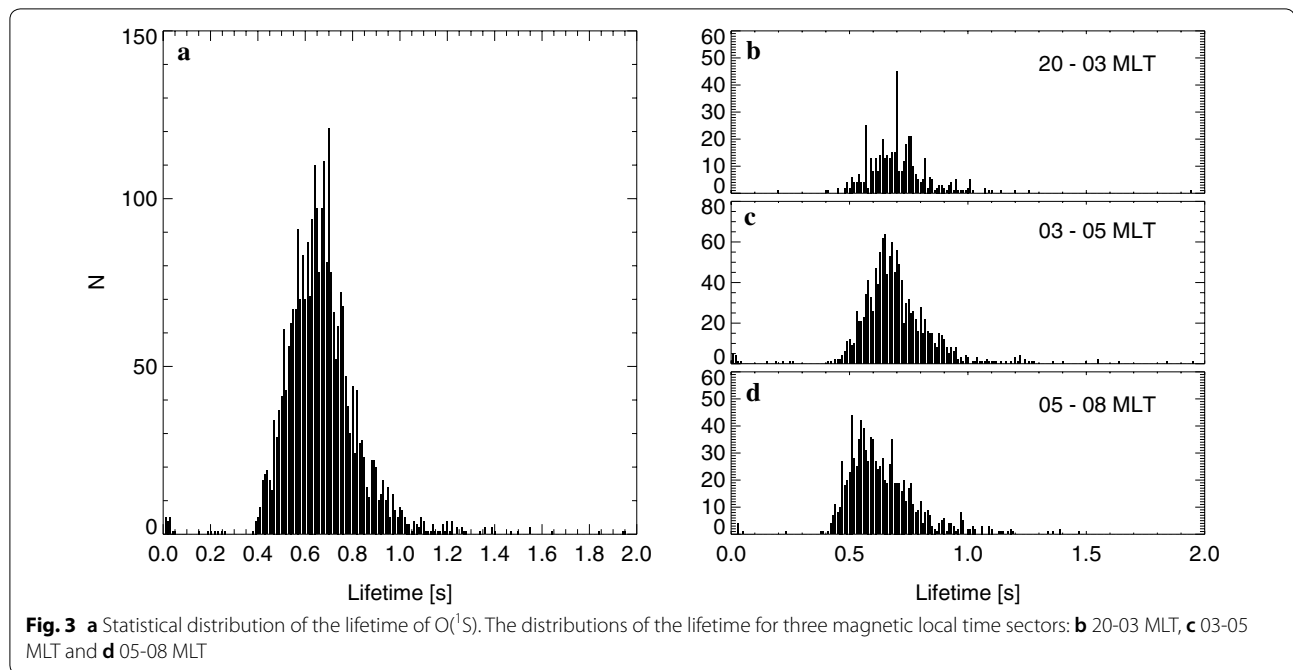
Here, we introduce a method to derive the altitude of the 557.7 nm emission from its lifetime (Scourfield et al. 1971). There are three routes through which an oxygen atom in the excited state transits to the ground state. Here, we define *I* as the intensity of 557.7 nm emission, which can be expressed as follows (Brekke and Henriksen 1972):

$$I = A_{32}/(A_{31} + A_{32} + d_3) \times Q_0$$

where *A*₃₁ and *A*₃₂ are the probability of radiative transition from O(¹S) state to O(¹D) and O(³P) states, respectively. *d*₃ is the probability of collisional transition of O(¹S) state. *Q*₀ is the excitation rate of O(¹S) state. Using these parameters, the lifetime of O(¹S) state is calculated as follows:

$$\tau = 1/(A_{31} + A_{32} + d_3).$$

In this equation, the values of *A*₃₁ and *A*₃₂ have been estimated experimentally and those are 1.28 s⁻¹ and 0.078 s⁻¹, respectively (Brekke and Henriksen 1972). Since we are able to estimate *τ* from actual observations of PsA, the collisional transition probability *d*₃ can be derived for each case of PsA. Assuming that there is no collisional transition of O(¹S) state, the lifetime is about 0.74 s. Therefore, when estimating the emission



altitude, we only used lifetime values which are less than or equal to 0.74 s.

Here, we assumed that the collisional transition is due to O₂ and N₂, and then d_3 can be expressed as follows:

$$d_3 = q_{O_2} \times n(O_2) + q_{N_2} \times n(N_2)$$

where q_{O_2} and q_{N_2} are the quenching rate coefficient of O₂ and N₂ and $n(O_2)$ and $n(N_2)$ are the density of O₂ and N₂, respectively. Using the theoretical value of q_{O_2} and q_{N_2} which are $3.0 \times 10^{-13} \text{ cm}^3 \text{ s}^{-1}$ (Zipf 1969) and $< 10^{-17} \text{ cm}^3 \text{ s}^{-1}$ (Hunten and McElroy 1966), the collisional transition due to N₂ can be ignored. Thus, d_3 can simply be expressed by the following equation (Scourfield et al. 1971):

$$d_3 = q_{O_2} \times n(O_2).$$

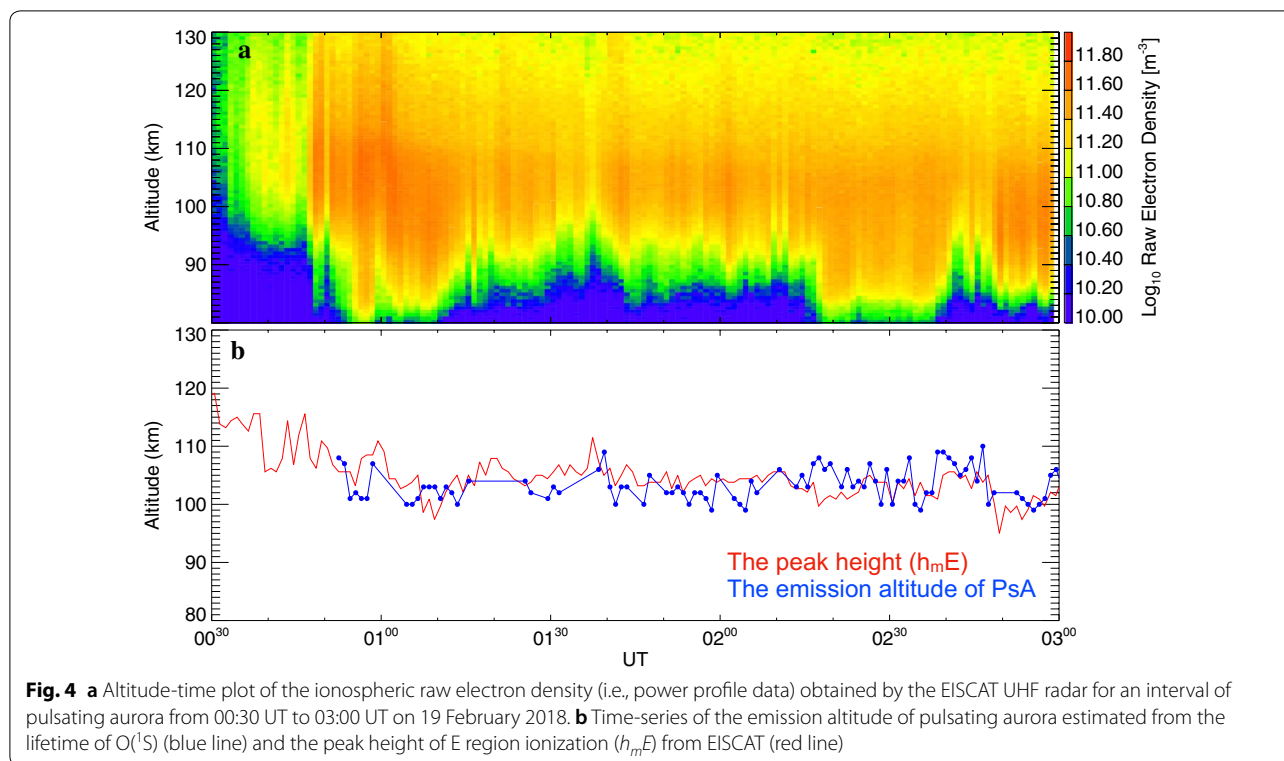
Using the theoretical value of q_{O_2} , we can determine the density of O₂ and then estimate the emission altitude of PsA by comparing the obtained value of $n(O_2)$ with that from the neutral atmosphere model [Mass Spectrometer and Incoherent Scatter: MSIS (Hedin 1991)] sampled every 1 km. The emission layer of PsA can be measured by incoherent scatter radar observations such as EISCAT, and its thickness is about 20 km (Jones et al. 2009; Hosokawa and Ogawa 2015). However, our method cannot directly estimate the lower cut-off altitude of the optical emission as well as the thickness of the emission layer. This is simply because it is difficult to obtain the height profile of the emission

from the optical observations. Therefore, we need to bear in mind that the emission altitude estimated in this study is the volume altitude which roughly means the center of the emission layer rather than the lower cut-off altitude.

Accuracy of estimating of the emission altitude

To evaluate the validity of the current method, here we compare the emission altitude of PsA estimated from the lifetime of O(¹S) and the altitude profile of the electron density from the EISCAT UHF radar whose FOV is $\sim 0.7^\circ$. The raw electron density (i.e., power profile data) was obtained with the altitude resolution of about 0.6 km. During 2.5 h from 00:30 to 03:00 UT on February 19, 2018, intense PsA and corresponding ionization were observed respectively by the five-wavelength photometer and the EISCAT UHF radar located in the same place. Figure 4a shows the variation of the ionospheric electron density from the EISCAT UHF radar. In this time interval, especially after 01:00 UT, PsA was observed by the photometer almost continuously. However, the low-altitude cut-off of ionization varied in time, which means that the characteristic energy of precipitating electrons was not uniform during this episode.

Figure 4b plots the time-series of the emission altitude of PsA derived from the lifetime analysis (blue line) and $h_m E$ (peak height of the E region electron density enhancement: red line). $h_m E$ has been derived directly from the altitude profile of the electron density shown in Fig. 4a. Note that we have averaged the original $h_m E$



values with a time window of 1 min to improve the signal-to-noise ratio.

Although there is a slight difference mainly due to the limited altitude resolution of $h_m E$, the altitude ranges of PsA emission and $h_m E$ are similar. In particular, during the 30 min from 02:30 to 03:00 UT, they show rather good agreement. This indicates that the emission altitude of PsA can be a good proxy for the energy of precipitating electrons during PsA.

Dependence of altitude of pulsating aurora on magnetic local time

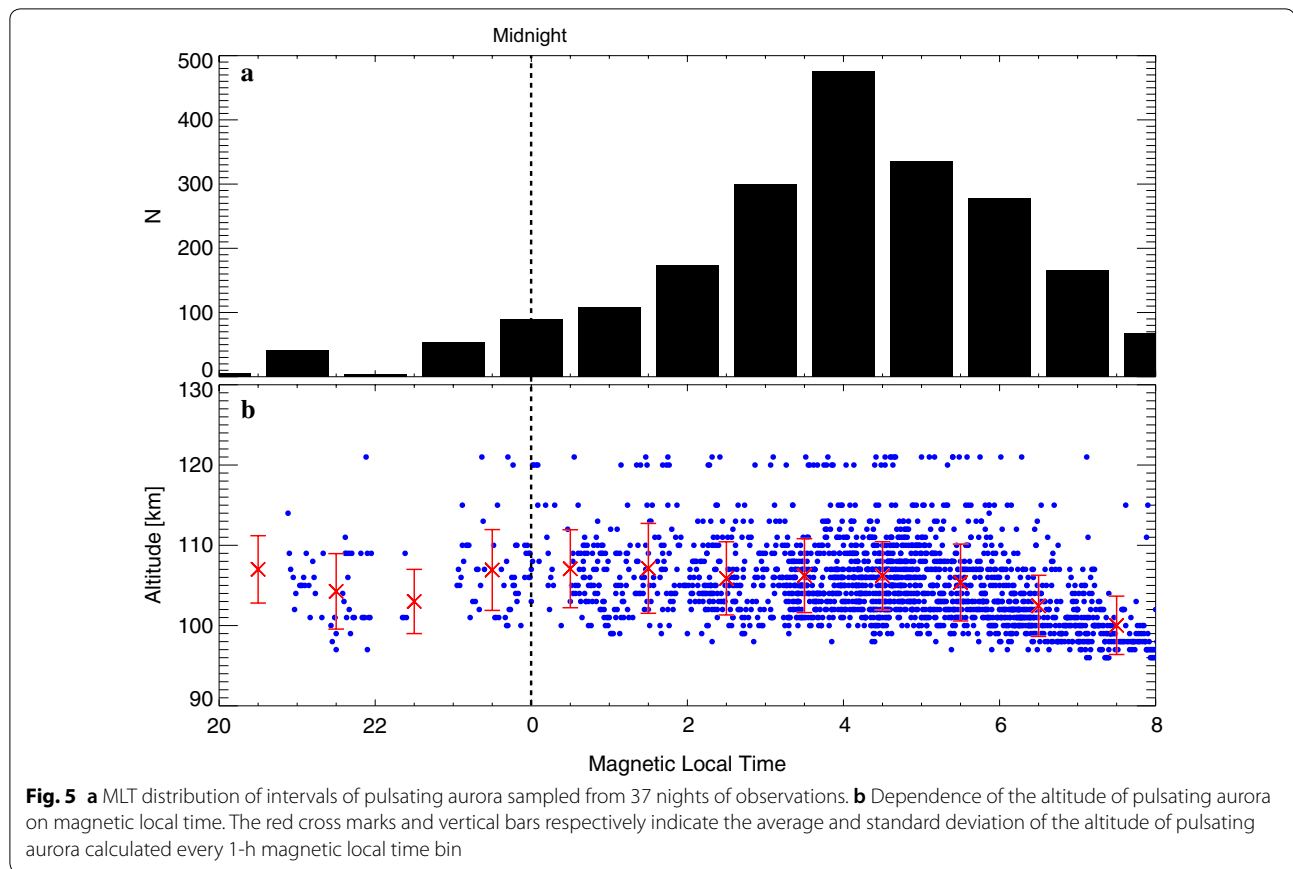
Figure 5a shows the MLT distribution of the occurrence of PsA events. Most events are distributed from the magnetic midnight to 08 MLT and the mode of distribution is located around 04 MLT. This distribution has good agreement with past studies of the occurrence distribution of PsA (e.g., Jones et al. 2011). Figure 5b shows the MLT variation of the emission altitude of PsA estimated in this study. Each dot corresponds to the emission altitude derived for each PsA interval. The red cross marks indicate the averages calculated every 1 h bin of MLT, and the red bars give the standard deviation of the distribution. The emission altitude becomes lower in the morning sector, especially after 06 MLT, while the central altitude stays high at around 108 km in the earlier MLT sector. After 06 MLT, the minimum emission altitude is

as low as ~ 95 km, which corresponds to the energy of precipitating electrons of 30 keV.

Discussion

As shown in Fig. 5b, the emission altitude of PsA is distributed in altitudes from 95 to 115 km, which corresponds to precipitation of 5–30 keV electrons (Turunen et al. 2009). This result is consistent with several early observations of PsA electrons by sounding rockets (Sandahl et al. 1980; Yau et al. 1981). Miyoshi et al. (2010, 2015b) also identified, using simultaneous particle and optical data from the Reimei satellite, precipitation of a few keV electrons causing PsA. Hosokawa and Ogawa (2015) investigated the variation of ionospheric electron density profile during PsA using the EISCAT radars and indicated that the energy of PsA electrons tends to be higher in the morning side. This tendency is actually seen in Fig. 5b, where the emission altitude drastically decreases after 06 MLT. This systematic change is consistent with the MLT variation of the E region peak height ($h_m E$) demonstrated by Hosokawa and Ogawa (2015). Similar MLT dependence has been reported by Partamies et al. (2017) who showed the MLT dependence of the emission layer of PsA.

Here, we discuss why the emission altitude of PsA decreases after 06 MLT. One of the possible explanations is the MLT change of the background magnetic field



intensity in the magnetosphere because the resonance energy of electrons in the first-order cyclotron resonant scattering with the chorus waves is proportional to the square of the ambient magnetic field intensity (Kennel and Petschek 1966):

$$E_R = \frac{B^2}{2\mu_0 N} \frac{f_{ce}}{f} \left(1 - \frac{f}{f_{ce}}\right)^3$$

where B is the ambient magnetic field intensity, μ_0 the permeability of a vacuum, N thermal plasma density, f_{ce} the cyclotron frequency, and f the frequency of chorus wave. Note that this approximation is valid when we assume $f_{pe}/f_{ce} \gg 1$ or $f/f_{ce} \ll 1$ (Kennel and Petschek 1966). Hosokawa and Ogawa (2015) have already calculated the magnetic field intensity and discussed the MLT variation of resonance energy. However, they have not yet evaluated the contribution of the thermal plasma density to the resonance energy.

Here, we calculated the magnetic field intensity at the conjugate point of Tromsø using the Tsyanenko 89 magnetic field model (Tsyanenko 1989) and the thermal plasma density using the model of Sheeley et al. (2001) for the PsA event on 19 February 2018. However, the

calculated value of resonance energy was almost uniform in MLT, implying that the drastic decrease of emission altitude cannot be explained only by the MLT change in the ambient parameters. Recently, Miyoshi et al. (2015a) pointed out that the resonance energy increases as the chorus wave propagates to higher latitude. If chorus waves propagate to higher latitude in the morning sector, more energetic electrons can be precipitated by the cyclotron resonance. Hence, the energy of PsA electrons should be discussed by considering both the ambient parameters (magnetic field intensity and thermal plasma density) and the propagation characteristics of chorus waves along the field line.

Conclusion

In this study, we estimated the emission altitude of PsA using the lifetime of $O(^1S)$ derived from the five-wavelength photometer in Tromsø, Norway. The main results are summarized as follows:

1. We have statistically analyzed the emission altitude of PsA using the observed value of lifetime of $O(^1S)$. The distribution of the lifetime has a strong peak at around 0.70 s and the mean lifetime is 0.67 s. These

automatically estimated time constants are in good agreement with those derived by the previous studies, implying the feasibility of the method for estimating the lifetime.

- Through comparison of the emission altitude of PsA with the peak height of the E region ionization obtained by the EISCAT UHF radar, we demonstrated that the peak height of electron density (i.e., peak of ionization) roughly matches the central emission altitude of PsA.
- There is a tendency that the emission altitude is significantly lower in the morning side after 06 MLT, suggesting that the energy of precipitating electrons should be higher at later MLT sector.

Abbreviations

PsA: Pulsating Aurora; PFIIR: Poker Flat Incoherent Scatter Radar; EISCAT: European Incoherent Scatter; EMCCD: Electron Multiplying Charged Coupled Device; FOV: field of view; UT: Universal Time; MLT: magnetic local time; MSIS: mass spectrometer and incoherent scatter; $h_m E$: the peak height of the electron density.

Acknowledgements

This work has been supported by Japan Society for the Promotion of Science (JSPS) JP 15H05747, 17H02968, JPJSBP12019814, 20H01959, and 20J12913. YK thanks the director and staff of EISCAT for operating the facility and supplying the data. EISCAT is an international association supported by research organizations in China (CRIPR), Finland (SA), Japan (ISEE and NIPR), Norway (NFR), Sweden (VR), and the United Kingdom (UKRI).

Authors' contributions

YK analyzed the data from the five-wavelength photometer and prepared the manuscript. SN and TK developed the five-wavelength photometer and carried out the observations. KH, SN, YO, SO, YM, and SK discussed the interpretation of the results. RF oversaw the observations and discussed the interpretation of the event. All authors contributed to completing the manuscript. All authors read and approved the final manuscript.

Funding

YK is supported by JSPS-Kakenhi (20J12913). YK and SO are supported by JSPS-Kakenhi (JPJSBP120194814). KH, YO, SO, YM, and RF are supported by JSPS-Kakenhi (15H05747). SN is supported by JSPS-Kakenhi (17H02968). SO is supported by JSPS-Kakenhi (16H06286, AF314664). YM is supported by JSPS-Kakenhi (15H05815, 16H06286, 17H00728, 20H01959).

Availability of data and materials

Data of EMCCD camera and the five-wavelength photometer from Tromsø are available through the ERG Science Center [(<https://ergsc.isee.nagoya-u.ac.jp/index.shtml>), Miyoshi et al. (2018)], ISEE, Nagoya University. Details can be found from the Kiban-S Web site at (<https://ergsc.isee.nagoya-u.ac.jp/psa-gnd/bin/psa.cgi>).

Ethics approval and consent to participate

Not applicable.

Consent for publication

Not applicable.

Competing interests

The authors declare that they have no competing interests.

Author details

¹ University of Electro-Communications, Chofugaoka 1-5-1, Chofu, Tokyo 182-8585, Japan. ² Institute for Space-Earth Environmental Research, Nagoya University, Furocho, Chikusa-ku, Nagoya, Aichi 464-8601, Japan. ³ National Institute of Polar Research, Midoricho 10-3, Tachikawa, Tokyo 190-8518, Japan. ⁴ Space Physics and Aeronomy Research Unit, University of Oulu, Pentti Kaiteran katu 1, Linnanmaa, 90014 Oulu, Finland. ⁵ Research Institute for Sustainable Humanosphere, Kyoto University, Uji, Kyoto 611-0011, Japan.

Received: 14 February 2020 Accepted: 2 July 2020

Published online: 10 July 2020

References

- Brekke A, Henriksen K (1972) The intensity ratio $I(5577)/I(4278)$ and the effective lifetime of $O(^1S)$ atoms in pulsating aurora. *Planet Space Sci* 20:53–60. [https://doi.org/10.1016/0032-0633\(72\)90140-7](https://doi.org/10.1016/0032-0633(72)90140-7)
- Brown NB, Davis TN, Hallinan TJ, Stenbaek-Nilsen HC (1976) Altitude of pulsating aurora determined by a new instrumental technique. *Geophys Res Lett* 7:403–404. <https://doi.org/10.1029/GL0031007p00403>
- Hedin AE (1991) Extension of the MSIS thermosphere model into the middle and lower atmosphere. *J Geophys Res* 96:1159–1172
- Hosokawa K, Ogawa Y (2015) Ionospheric variation during pulsating aurora. *J Geophys Res* 120:5943–5957. <https://doi.org/10.1002/2015JA021401>
- Hosokawa K, Miyoshi Y, Li W (2015) Introduction to special section on pulsating aurora and related magnetospheric phenomena. *J Geophys Res* 120:5341–5343. <https://doi.org/10.1002/2015JA021453>
- Hosokawa K, Miyoshi Y, Ozaki M, Oyama SI, Ogawa Y, Kurita S, Kasahara Y, Kasaba Y, Yagitani S, Matsuda S, Tsuchiya F, Kumamoto A, Kataoka R, Shiokawa K, Raita T, Turunen E, Takashima T, Shinohara I, Fujii R (2020) Multiple time-scale beats in aurora: precise orchestration via magnetospheric chorus waves. *Sci Rep* 10:3380. <https://doi.org/10.1038/s41598-020-59642-8>
- Hunten DM, McElroy MB (1966) Quenching of metastable states of atomic and molecular oxygen and nitrogen. *Rev Geophys* 4(3):303–328. <https://doi.org/10.1029/RG004i003p00303>
- Jones SL, Lessard MR, Fernandes PA, Lummerzheim D, Semeter JL, Heinselman CJ, Lynch KA, Michell RG, Kintner PM, Stenbaek-Nielsen HC, Asamura K (2009) PFIIR and ROPA observations of pulsating aurora. *J Atmos Sol Terr Phys* 71:708–716. <https://doi.org/10.1016/j.jastp.2008.10.004>
- Jones SL, Lessard MR, Rychert K, Spanswick E, Donovan E (2011) Large scale aspects and temporal evolution of pulsating aurora. *J Geophys Res* 116:A03214. <https://doi.org/10.1029/2010JA015840>
- Kasahara S et al (2018) Pulsating aurora from electron scattering by chorus waves. *Nature* 554(7692):337–340. <https://doi.org/10.1038/nature25505>
- Kennel CF, Petschek HE (1966) Limit on stably trapped particle fluxes. *J Geophys Res* 71(1):1–28. <https://doi.org/10.1029/JZ071i001p00001>
- Kvifte GJ, Pettersen H (1969) Morphology of the pulsating aurora. *Planet Space Sci* 17:1599–1607. [https://doi.org/10.1016/0032-0633\(69\)90148-2](https://doi.org/10.1016/0032-0633(69)90148-2)
- Miyoshi Y, Katoh Y, Nishiyama T, Sakanoi T, Asamura K, Hirahara M (2010) Time of flight analysis of pulsating aurora electrons, considering wave–particle interactions with propagating whistler mode waves. *J Geophys Res* 115:A10312. <https://doi.org/10.1029/2009JA015127>
- Miyoshi Y et al (2015a) Energetic electron precipitation associated with pulsating aurora: EISCAT and Van Allen Probe observations. *J Geophys Res Space Phys* 120:2754–2766. <https://doi.org/10.1002/2014JA020690>
- Miyoshi Y, Saito S, Seki K, Nishiyama T, Kataoka R, Asamura K, Katoh Y, Ebihara Y, Sakanoi T, Hirahara M, Oyama S, Kurita S, Santolik O (2015b) Relation between energy spectra of pulsating aurora electrons and frequency spectra of whistler-mode chorus waves. *J Geophys Res* 120:7728–7736. <https://doi.org/10.1002/2015JA021562>
- Miyoshi Y, Hori T, Shoji M, Teramoto M, Chang T-F, Segawa T, Umemura N, Matsuda S, Kurita S, Keika K, Miyashita Y, Seki K, Tanaka Y, Nishitani N, Kasahara S, Yokota S, Matsuoka A, Kasahara Y, Asamura K, Takashima T, Shinohara I (2018) The ERG Science Center. *Earth Planets Space* 70:96. <https://doi.org/10.1186/s40623-018-0867-8>
- Nishimura Y et al (2010) Identifying the driver of pulsating aurora. *Science* 330:81–84. <https://doi.org/10.1126/science.1193186>

- Nishimura Y et al (2011) Multievent study of the correlation between pulsating aurora and whistler mode chorus emissions. *J Geophys Res* 116:A11221. <https://doi.org/10.1029/2011JA016876>
- Nozawa S, Kawabata T, Hosokawa K, Ogawa Y, Tsuda T, Mizuno A, Fujii R, Hall C (2018) A new five-wavelength photometer operated in Tromsø (69.6°N, 19.2°E). *Earth Planets Space* 70:193. <https://doi.org/10.1186/s40623-018-0962-x>
- Partamies N, Whiter D, Kadokura A, Kauristie K, Nesse Tyssøy H, Massetti S et al (2017) Occurrence and average behavior of pulsating aurora. *J Geophys Res* 122:5606–5618. <https://doi.org/10.1002/2017JA024039>
- Royrvik O, Davis TN (1977) Pulsating aurora: local and global morphology. *J Geophys Res* 82(29):47204740. <https://doi.org/10.1029/JA082i029p04720>
- Sandahl I, Eliasson L, Lundin R (1980) Rocket observations of precipitating electrons over a pulsating aurora. *Geophys Res Lett* 7(5):309312. <https://doi.org/10.1029/GL007i005p00309>
- Sato N, Wright DM, Carlson CW, Ebihara Y, Sato M, Saemundsson T, Milan SE, Lester M (2004) Generation region of pulsating aurora obtained simultaneously by the FAST satellite and a Syowa-Iceland conjugate pair of observatories. *J Geophys Res* 109:A10201. <https://doi.org/10.1029/2004JA010419>
- Scourfield MWJ, Parsons NI, Dennis LP, Innes WF (1971) Effective lifetime of O(¹S) in Pulsating Aurora. *J Geophys Res* 76:3692–3699. <https://doi.org/10.1029/JA076i016p03692>
- Sheeley BW, Moldwin MB, Rassoul HK, Anderson RR (2001) An empirical plasmasphere and trough density model: CRRES observations. *J Geophys Res* 106:25631–25641
- Tsyganenko NA (1989) A magnetospheric magnetic field model with a warped tail current sheet. *Planet Space Sci* 37:5–20. [https://doi.org/10.1016/0032-0633\(89\)90066-4](https://doi.org/10.1016/0032-0633(89)90066-4)
- Turunen E, Verronen PT, Seppala A, Rodger CJ, Clilverd MA, Tamminen J, Enella C-F, Ullrich T (2009) Impact of different energies of precipitating particles on NO_x generation in the middle and upper atmosphere during geomagnetic storms. *J Atmos Sol Terr Phys* 71:1176–1189
- Yamamoto T (1988) On the temporal fluctuations of pulsating auroral luminosity. *J Geophys Res* 93:897911. <https://doi.org/10.1029/JA093iA02p00897>
- Yau AW, Whalen BA, McEwen DJ (1981) Rocket-borne measurements of particle pulsation in pulsating aurora. *J Geophys Res* 86:5673–5681. <https://doi.org/10.1029/JA086iA07p05673>
- Zipf EC (1969) The collisional deactivation of metastable atoms and molecules in the upper atmosphere. *Can J Chem* 47:1863

Publisher's Note

Springer Nature remains neutral with regard to jurisdictional claims in published maps and institutional affiliations.

Submit your manuscript to a SpringerOpen[®] journal and benefit from:

- Convenient online submission
- Rigorous peer review
- Open access: articles freely available online
- High visibility within the field
- Retaining the copyright to your article

Submit your next manuscript at ► [springeropen.com](https://www.springeropen.com)
